Light-sheet enhanced resolution of light field microscopy for rapid imaging of large volumes

Jorge Madrid-Wolff [a,b], Diego Castro[a], Pablo Arbeláez[b], Manu Forero-Shelton[a,*]

[a] Biophysics Laboratory, Universidad de los Andes, Bogota, Colombia; [b] Biomedical Computer Vision Group, Universidad de los Andes, Bogota, Colombia.

*anforero@uniandes.edu.co

Abstract

Whole-brain imaging is challenging because it demands microscopes with high temporal and spatial resolution, which are often at odds, especially in the context of large fields of view. We have designed and built a light-sheet microscope with digital micromirror illumination and light-field detection. On the one hand, light sheets provide high resolution optical sectioning on live samples without compromising their viability. On the other hand, light field imaging makes it possible to reconstruct full volumes of relatively large fields of view from a single camera exposure; however, its enhanced temporal resolution comes at the expense of spatial resolution, limiting its applicability. We present an approach to increase the resolution of light field images using DMD-based light sheet illumination. To that end, we develop a method to produce synthetic resolution targets for light field microscopy and a procedure to correct the depth at which planes are refocused with rendering software. We measured the axial resolution as a function of depth and show a three-fold potential improvement with structured illumination, albeit by sacrificing some temporal resolution, also three-fold. This results in an imaging system that may be adjusted to specific needs without having to reassemble and realign it. This approach could be used to image relatively large samples at high rates.

Keywords: Light field microscopy, light sheet fluorescence microscopy, resolution enhancement, structured illumination, Digital Micromirror Device

1. INTRODUCTION

Recent progress in fluorescent indicators such as calcium markers and transgenic model organisms has allowed the study of rapid dynamic biological processes in vivo like neural signaling, cardiovascular activity, and bacterial populations. Still, current imaging techniques have limitations to study these processes because of the trade-off between spatial resolution and temporal resolution. Confocal microscopy has good resolution but records images sequentially voxel by voxel in each slice and slice by slice, making it too slow to understand dynamic processes in three dimensions. Light Sheet Fluorescence Microscopy (LSFM) which also has good resolution and is more efficient light-wise, records individual slices in parallel making it orders of magnitude faster[1], still since different sections are recorded sequentially, its detection speed is limited by how fast the sample or the detection objective can be moved. Progress has been achieved using high speed and sensitivity CMOS cameras and power piezo translators for either the detection objective or the sample, but for example in the case of whole-brain electrical activity in zebrafish embryos the speed is in the order of about a whole brain volume per second, which may miss many aspects related to the timing of brain activity[2]. Other methods to increase the speed include electrically tunable lenses[3] and extended depth of field via spherical aberration[4] or wavefront coding[5,6], but they have only been shown in sparse neural networks.

Imaging large volumes under LSFM is limited by the speed of its sequential plane acquisition. Light field imaging, on the other hand, acquires a single volume in parallel, with a single exposure of the camera. However, this high temporal resolution comes at the cost of spatial resolution. Light field microscopy has been used to image neural activity in live

Three-Dimensional and Multidimensional Microscopy: Image Acquisition and Processing XXV, edited by Thomas G. Brown, Carol J. Cogswell, Tony Wilson, Proc. of SPIE Vol. 10499, 104991U
 · doi: 10.1117/12.2290188

embryos[7,8] and fluid dynamics[9], for instance. So far, in the context of neural activity, it has been possible to follow the activity of neural structures for sparse neuron distributions[8].

For light field imaging, limited resolution is a consequence of the limited available information that can be read by the detector. Any enhancement of the spatial resolution either attempts to optimize the way in which information is used in the imaging process or attempts to include additional information in the reconstruction. Approaches attempting to optimize the use of information encompass the enhancement of angular resolution based on the local estimation of disparity maps[10], which have proven useful for macroscopic light field photography but where specimens are transparent, disparity maps have little significance. Approaches attempting to incorporate additional information include calculated PSF-based deconvolution[11], computational super-resolution methods in which ground-truth orthographic images are used as targets for the optimization of image interpolation[12], and merging complementary light fields through graph regularization[13],; and the imposition of constraints on certain features of the reconstruction, such as texture[14], which is also useful in photography but meaningless in microscopy. Between the two general approaches, we opt for the addition of new information, but we highlight the need to incorporate it rapidly.

Lateral resolution changes as a function of depth in light field microscopes, and this has been characterized previously[15], showing that it is reduced away from the focal plane of the detection objective and at the focal plane itself, similar to a cardioid around the focal depth, unless phase masks are used[16]. Yet little is known about axial resolution in a light field microscope and, to our best knowledge, no previous work has fully characterized its dependence on depth.

Here, we explore the potential of light sheet and light field microscopy used in a complementary manner in order to gain spatial resolution in the axial direction of the detector objective (defined as z here) with respect to traditional light field microscopy, and in a way that should result in improved temporal resolution with respect to LSFM. We incorporate light field detection to a light sheet microscope that uses a digital micromirror device (DMD) to project illumination planes on the sample. In order to improve the spatial resolution of the detection depth, we propose to structurally illuminate the sample with light sheets separated more than the axial resolution of the detection. We make use of our light sheet illumination to study the dependence of axial resolution on depth in light field microscopy. We propose to image the full volume in several exposures of the camera, each corresponding to one set of resolvable planes.

2. METHODS

2.1. Optical set-up

We built a light field microscope in which we could selectively illuminate certain planes in the sample, as shown in figure 1. To this end, we combined a light sheet and a light field microscope. In our setup, light from a 488nm 200mW diode laser (Cobolt, 06-MLD) was directed onto a digital micromirror device (Texas Instruments, DLPLCR6500EVM). Each light sheet was formed by turning on a vertical fringe on the DMD and projected onto the sample via a 200mm tube lens and the illumination objective (either a 20x 0.6 NA from Edmund Optics or a Leica 10x 0.25). Our test samples consisted of 2μm fluorescent beads suspended in an agarose cylinder hanging from a glass capillary.

An Olympus LUMFLN 60XW 1.1 NA water immersion objective collected the fluorescence from the micrometric beads. The orthographic detection arm of the microscope serves for inspection and sample navigation, as getting oriented in light field captures is not necessarily intuitive. This detection system consisted of an f=100mm achromat and an sCMOS camera. The light field detection included a band-pass filter to reject light from the illumination. Then, we used an f=150mm achromat as the tube lens focusing the light on an f/#=21, Ø=100μm microlens array (RPC photonics), closely matching the f-number in the detection arm. We translated the back focal plane of the microlenses onto the sensor of a Hamamatsu ORCA-Flash4.0 V2 digital CMOS camera by means of an M=1 relay pair.

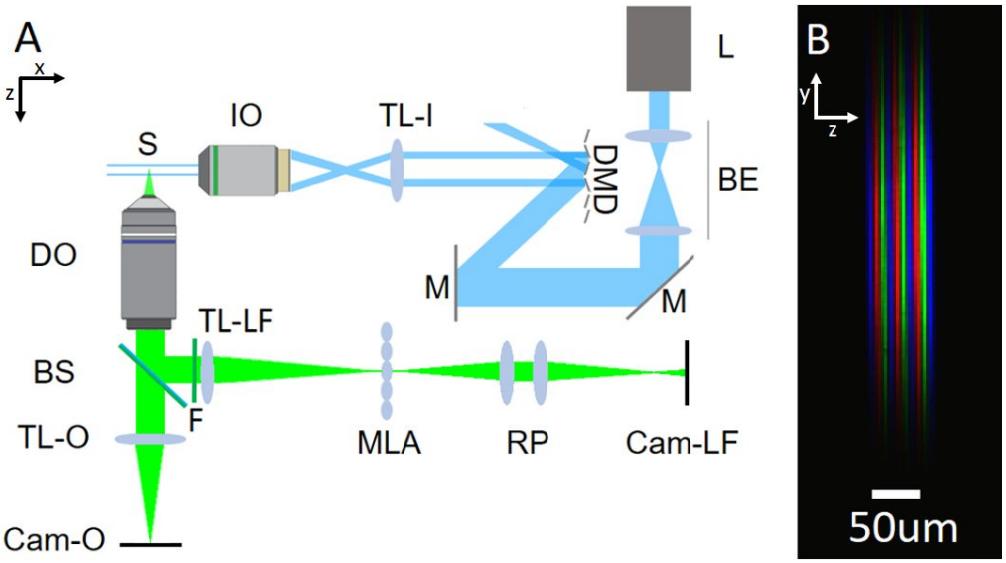

Figure 1. Optical set-up. A) A light sheet light field microscope is built by adding light field detection to a DMD-based light sheet illumination microscope. The beam from a laser (L) is rescaled in a beam expander (BE. The beam is then directed at a specific angle onto a (DMD). Following a digital pattern transferred from a computer, the DMD redirects and discards light to form an illumination pattern. The illumination tube lens (TL-I) and objective (IO) project an image of the illumination pattern on the sample (S). A sample of fluorescent beads is placed in front of the IO while a perpendicular detection objective (DO) collects the emitted light from the sample. A long-pass dichroic beam splitter (BS) transmits the tail of the emitted fluorescence, which forms an image at the orthographic detection by means of a tube lens (TL-O) and a camera (Cam-O). The light field detection collects the reflected light from BS and filters it with a band-pass filter (F) to reject illumination light. Light is then focused by a tube lens (TL-LF) onto a microlens array (MLA). The back focal plane of the microlenses is translated by a relay pair (RP) onto a digital camera (Cam-LF). **B)** Pseudo-color image of a structured illumination pattern of three-mirror wide vertical fringes with seven-mirror spacings between them. This photograph was acquired at the focal plane of the illumination objective. Colors indicate time of illumination, as in figure 5.

2.2. Image processing and light field reconstructions

We developed light field rendering software that returned focal stacks, i.e. a collection of synthetically refocused planes corresponding to the imaged volume. We followed the algorithm presented by Ng *et al*[17]. Light field rendering requires reshaping the data contained in a two-dimensional light field capture into a four-dimensional tensor. We show the steps we followed to process the light field below.

Initial image processing

First, it is necessary to carefully align the position of each microlens with respect to the pixels of the camera's sensor. During microscope alignment we mounted the microlens array on a 6-axis kinematic mount (able to rotate the microlenses) in order to have the array coincide with the pixels of the camera as well as possible, in terms of positions and angles. Further corrections were done by digitally rotating the sensor image. Once the coordinate systems of both pixels and microlenses were aligned, we found the spatial period, in pixel units, of the microlenses. We found the vertical and horizontal periods of the microlenses by adding the intensities of the image along rows and columns of pixels, respectively, and then computing the Fourier transform of these summations. We kept the frequencies with the maximal powers and fed them as starting points for ω to the optimization of the function

$$microlens\ position = A\cos(\omega x + x_0) + C$$

This optimization returned a finer measurement of the spatial period of the microlenses with respect to the pixels. Finally, we rescaled the light field capture so that the spatial periods of the microlenses were integer multiples of pixels.

Synthetic refocusing

We generated focal stacks by iterating over the refocusing parameter α as defined in [17], and solving the discrete version of the integral, presented in [18],

$$E'(x',y') = \iint L\left(\left(\frac{\alpha-1}{\alpha}\right)(u-R)+x', \left(\frac{\alpha-1}{\alpha}\right)(v-R)+y', u, v\right) dudv \qquad (1).$$

Where *E'* is the intensity on the synthetic plane, *u* and *v* are the horizontal and vertical microlens coordinates, *x´* and *y´* are the horizontal and vertical coordinates for a pixel in the refocused plane, *L* is the light field tensor, *R* is the microlens radius in pixels, and α is the refocusing parameter which determines the plane *F',* located at a distance *z* from the focal plane *F,* on which light rays are refocused by the integral. The refocusing parameter α is defined as follows:

$$\alpha = \frac{F'}{F} = \frac{F+z}{F} \qquad (2).$$

Synthetic refocusing may be understood as a summation over the light field tensor, as expressed by equation 1, from the fact that by inserting the microlens array, we spread light rays over various pixels on the camera sensor. Thus, when reconstructing the intensity for a given pixel on the new synthetic plane, we intend to sum the intensities of all the light rays that originated from that point in space and that were recorded by the sensor. As all those light rays intersect on that point, their *x*, *y* coordinates may be expressed in terms of *u* and *v* and some indication of the position of the intersecting point, namely the refocusing parameter α.

2.3. Calibration of the refocusing parameter α

For a small range of depths, we found that α was essentially linear with depth; it was not linear over a larger range. Thus, we found it necessary to evaluate the experimental dependence of α on *z* along a depth range of over 100μm. We used a collection of light field captures of single microspheres placed at known depths using a micromanipulator and produced a focal stack for each light field capture. We extracted the intensity profile for each stack along the *z*-axis and through the center of the PSF. We then found the depth of maximal intensity, which was the depth at which the microsphere had been localized in the light field reconstruction. We noticed that for intermediate depths between 30 and 60μm, α exhibited a linear dependence on *z,* as described by eq. 2. However, over the range of 0 to 100μm, α was better described by the arctangent of *z*, displaying an asymptotic behavior towards the end of the depth range, as shown in figure 2. This factor may contribute to the degradation of resolution at large depths.

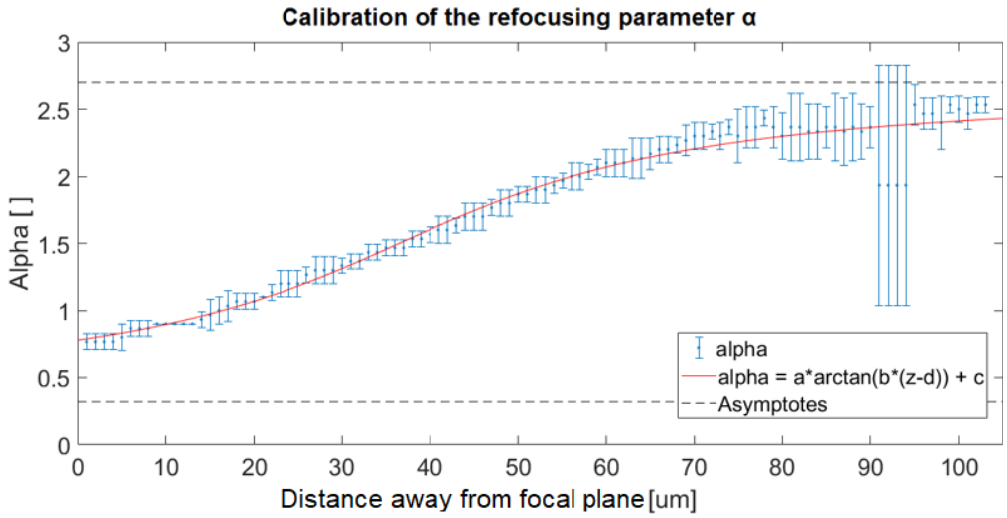

Figure 2. Calibration of the refocusing parameter *α*. Experimental calibration of the refocusing parameter alpha as a function of the depth of the plane of interest, *α(z)*. *α* only exhibits the expected linear dependence on *z* within a relatively narrow depth range from about 30 to 60µm. *α* is better described as the arctangent of the depth, resulting in an asymptotic behavior for planes farther away from the focus. Such asymptotic behavior limits the depth range of values of *α* needed to reconstruct a full volume.

2.4. Production of synthetic resolution targets

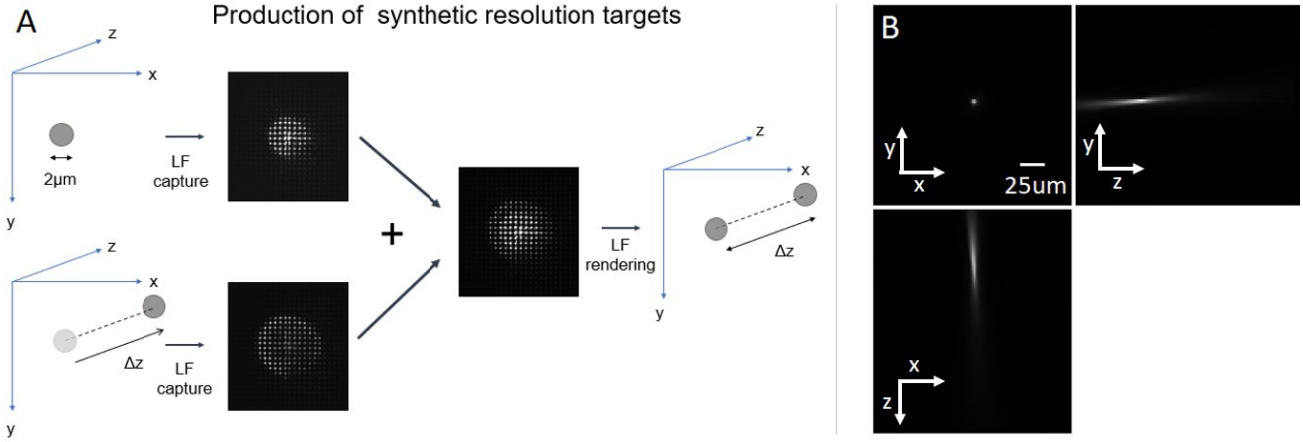

Figure 3. Production of synthetic resolution targets. A. We produced synthetic resolution targets by acquiring the light field of a single fluorescent microsphere in the field of view and then displacing the microsphere a known distance Δz along the *z*-axis to acquire a second light field. We then added the two light field captures and used the resulting image to render a volume. The rendered volume corresponded to a view of two microspheres separated Δz. **B.** Orthographic projections for the rendered volume of a single microsphere.

In order to obtain an initial estimate of the resolution of the system along the *z*-axis, we recorded light fields of volumes of a single 2µm fluorescent microsphere at different depths and added the intensities of both images. By combining the intensities at the sensor from two light field exposures from different depths it is possible to get an estimate of the best resolution for the spheres within this depth range, at least for our reconstruction algorithm. This process is illustrated in

figure 3. Once a simple reconstruction was achieved, we averaged the intensities of 3 voxels in the y-direction that contained the bead, and plotted this along z in order to measure resolution. We established a criterion for resolution in the following way, essentially a Rayleigh criterion: we fit the intensity cross sections in z along the center of the beads in the reconstruction and fit those to two airy functions using a Matlab script. The beads at different depths were resolvable if the first minima of each airy function was at least at the maximum of the other airy function. It is important to do this for both airy functions since their width may not be the same.

3. RESULTS

3.1. Axial resolution dependence on depth

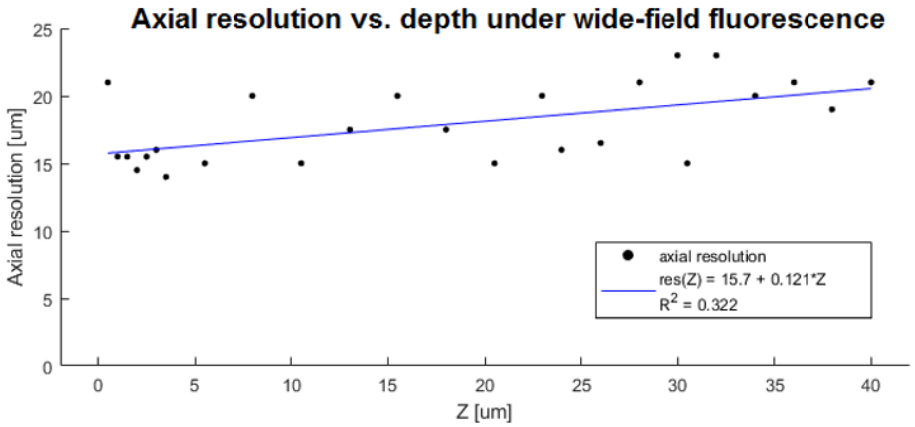

Figure 4. Axial resolution as a function of depth under wide-field side-illumination fluorescence. The ability of a light field microscope to resolve light sources at different depths has an apparent dependence on depth. Z refers to the depth position of the microsphere closest to the focal plane. Z = 0 corresponds to the focal plane. Lower is better.

In order to be able to quantify any resolution improvements under a structured illumination scheme, we first calculated the resolution of the system as a function of depth, using synthetic resolution targets as described in the methods section. In brief, we combined the intensities from the images of a pair of beads at different depths and after a simple reconstruction without deconvolution, we defined that the two beads could be resolved if the minimum of the fit of airy functions for each bead was at least as far as the maximum of the other bead. For each depth, we tested how far a second bead had to be from that particular depth in order to be resolved, and report this minimum distance. Figure 4 shows the dependence of the axial resolution on depth. In this figure, Z refers to the depth of the microsphere closest to the focal plane; as expected *z*-resolution worsens as we get away from the focal plane, i.e., as the sample sits closer to the objective. This is comparable to the results obtained by Cohen *et al.*[16]

3.2. Potential of axial resolution improvement with structured illumination

In order to estimate potential gains in resolution, instead of observing two beads, we built a synthetic arrangement consisting of six 2µm polyethylene fluorescent microspheres separated by 4,5µm from each other along the *z*-axis behind each other, as in figure 5. We placed the first microsphere at z=13.5µm. We know from figure 4 that neighboring microspheres sitting this close may not be resolvable under wide field illumination light field microscopy. However, these six microspheres may be viewed as three pairs of beads, with the two beads distanced 13,5µm. At this distance two beads are close to being resolved according to Figure 4. Since, as shown in figure 1B we were able to generate light sheets approximately 4µm wide at the focal plane, it should be possible to illuminate the sample with sheets thin enough to avoid illuminating more than one bead at a time. To establish if it is possible to resolve the six beads with a structured illumination scheme, we decided to use three illumination phases, each illuminating two beads. The enhancement of

axial resolution comes, however, at the cost of temporal resolution since we would have to expose the sample three times.

Figure 5 shows that under this structured light sheet illumination scheme, beads within each exposure could be resolved. Note that for the exposure of the beads further from the focal plane, beads were not resolvable by our criterion, although a dip in their combined intensity profile can be easily appreciated. In contrast, when the six beads were illuminated simultaneously under wide-field illumination black dots, it was impossible to distinguish the beads. This indicates that our proposed method of light-sheet-light-field structured-illumination microscopy does enhance axial resolution around three-fold (4.5 microns instead of 15), which is essentially as much as the time penalty. Note that in order to reconstruct this volume we would have to use the fits and re-localize the fluorescence intensity to the planes we know are illuminated, with the particular width of the light sheet with which it was illuminated.

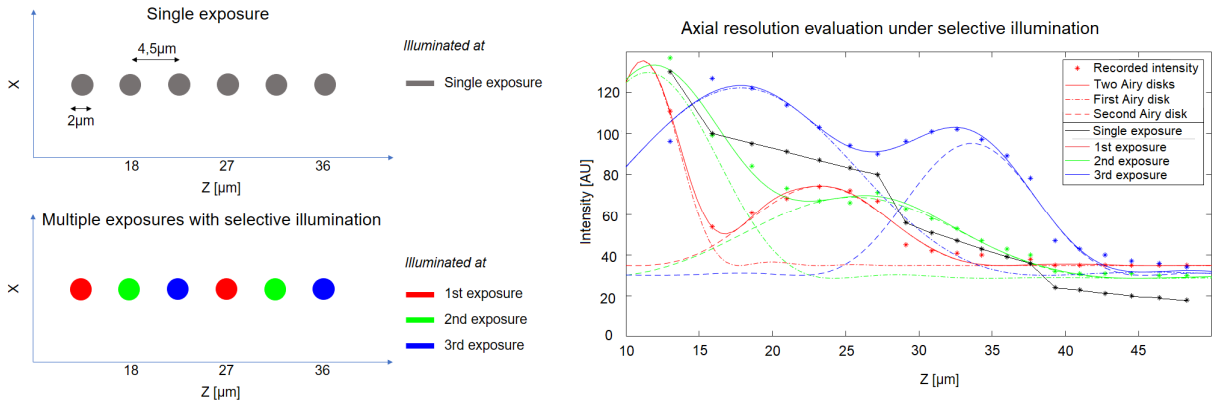

Figure 5. Axial resolution in a synthetic sample composed of closely spaced light sources. *(Left top)* A synthetic sample of six 2µm polyethylene fluorescent microspheres is produced and rendered as if all beads were illuminated simultaneously. Under this illumination, neighboring beads separated by 4,5µm are not resolvable. *(Left bottom)* Synthetic light fields are produced emulating the selective illumination of the six beads in three exposures, each containing two lit beads and four unlit beads. Under this illumination, neighboring beads in one exposure sit 13,5µm apart. A sacrifice of temporal resolution has been made in favor of axial resolution. (*Right)* Intensity profiles of the reconstructed volume corresponding to *Left top* in black, in which the six beads are not resolvable, and to the three reconstructions corresponding to *Left bottom,* in which the pairs of beads are resolvable (except for the third exposure). The fits to the Airy disks are included to show that the beads are indeed resolvable.

4. DISCUSSION

We built a light sheet light field microscope with which it is possible to illuminate a sample using a DMD. We were able to produce multiple light sheets at different depths, and it should be possible to vary their separation and width according do different needs and structure them to illuminate a sample. We measured how the axial resolution of the system changed with depth in our optical setup under wide-field fluorescence. We compared this resolution with the one that could be obtained when illuminating the sample in a synthetic experiment and demonstrated an axial resolution improvement from ~15µm to ~4.5µm (i.e by about three-fold) while reducing temporal resolution also three-fold. This is of special interest because the improvement in axial resolution is not more than the sacrifice in temporal resolution, making a system based in this technology flexible according to the experimental needs in spatial and temporal resolution. We also experimentally calibrated the refocusing parameter α in our software in order to correctly refocus planes over large depths and evidenced its non-linearity over large depth ranges. The DMD is also interesting in this context as resolution is not constant with depth, decreasing away from the focal plane. Given these two limitations, it should be

possible to adjust the spacing between the light sheets generated by the DMD in order to compensate or the non-linearity of the reconstruction and the changes (and necessities) in resolution with depth.

The structured light sheet illumination presented here could be useful to give flexibility and/or improve the resolution of other methods that are able to obtain high-resolution images at multiple depths such as extended depth of field or multifocus microscopy [19,20]. Multifocus Microscopy projects different depths of a sample on different parts of the camera's sensor using a diffractive element, sacrificing field of view and limiting the emission bandwidth of the fluorophores. However, for the imaging of large fields of view, larger cameras, or tiled cameras such as those used in astronomy would be necessary. We expect our approach to be more flexible and adaptable, enabling the use of one instrument across different samples, either with light field detection or other extended depth of field detection method, by effectively making samples sparser.

The field of view for the light field detection at the focal plane is of roughly $250\mu m x 250\mu m$. Although the field of view decreases as we image planes further from the focal plane, the estimated observable volume of $250\mu m x 250\mu m x 100\mu m$ works well for imaging *C elegans*, large sections of the larval zebrafish brain, or a good portion of *Drosophila* embryos, for instance. Given the flexible design of the technique, a light sheet light field microscope could be readily adapted to image different samples.

A significant limitation of the illumination method is that a large portion of the power to illuminate the sample is wasted for each individual micromirror that is on the off state. This could be resolved by using diffractive elements and galvo scanners, at the expense of flexibility. Moreover, the whole power is, by design, distributed among various light sheets, further increasing the need for higher intensity lasers.

5. CONCLUSIONS

In this work we measure the dependence on depth of the axial resolution of a light field microscope under wide-field fluorescence illumination and its subsequent enhancement thanks to selective-plane illumination using light sheets by means of synthetic resolution targets. We demonstrate that a three-fold enhancement of the axial resolution of the microscope can be achieved in a dense sample (in the z direction) by reducing temporal resolution to a third. We also evaluate the dependence on depth of the refocusing parameter used in light field rendering software and demonstrate that it must be experimentally calibrated when deep volumes are to be imaged. In future work we expect to validate the method with animal samples as well as its temporal resolution in those samples.

6. ACKNOWLEDGEMENTS

The authors thank Luis Gómez and his team for building custom parts for the optical setup, Jhonny Turizo for developing support software and electronics, RealLabs for designing and implementing control software, Angela Narváez for contributing to the alignment of the setup, and Nicolás Barbosa for helping with data acquisition.

Manu Forero-Shelton acknowledges the equipment as well as the consumables grants from the Department of Physics, Universidad de los Andes. We also thank the groups intramural grant on survival mechanisms of pathogens, a grant from Colciencias 120471250721. He also acknowledges Guillaume Gay for help in the initial microscope´s design. Software under license from Howard Hughes Medical Institute, Janelia Farm Research, served as inspiration for the development of control software implemented for the prototype microscope used in this work.

REFERENCES

[1] Huisken, J., Swoger, J., Del Bene, F., Wittbrodt, J., and Stelzer, E.H.K., "Optical Sectioning Deep Inside Live Embryos by Selective Plane Illumination Microscopy," Science 305(5686), 1007–1009 (2004).

[2] Ahrens, M.B., Orger, M.B., Robson, D.N., Li, J.M., and Keller, P.J., "Whole-brain functional imaging at cellular resolution using light-sheet microscopy," Nature Methods 10(5), 413–420 (2013).

[3] Fahrbach, F.O., Voigt, F.F., Schmid, B., Helmchen, F., and Huisken, J., "Rapid 3D light-sheet microscopy with a tunable lens," Optics Express 21(18), 21010–21026 (2013).

[4] Tomer, R., Lovett-Barron, M., Kauvar, I., Andalman, A., Burns, V.M., Sankaran, S., Grosenick, L., Broxton, M., Yang, S., et al., "SPED Light Sheet Microscopy: Fast Mapping of Biological System Structure and Function," Cell 163(7), 1796–1806 (2015).
[5] Olarte, O.E., Andilla, J., Artigas, D., and Loza-Alvarez, P., "Decoupled illumination detection in light sheet microscopy for fast volumetric imaging," Optica 2(8), 702 (2015).
[6] Quirin, S., Vladimirov, N., Yang, C.-T., Peterka, D.S., Yuste, R., and Ahrens, M., "Calcium imaging of neural circuits with extended depth-of-field light-sheet microscopy," Optics Letters 41(5), 855 (2016).
[7] Prevedel, R., Yoon, Y.-G., Hoffmann, M., Pak, N., Wetzstein, G., Kato, S., Schrödel, T., Raskar, R., Zimmer, M., et al., "Simultaneous whole-animal 3D imaging of neuronal activity using light-field microscopy," Nature Methods 11(7), 727–730 (2014).
[8] Pégard, N.C., Liu, H.-Y., Antipa, N., Gerlock, M., Adesnik, H., and Waller, L., "Compressive light-field microscopy for 3D neural activity recording," Optica 3(5), 517–524 (2016).
[9] Truscott, T.T., Belden, J., Ni, R., Pendlebury, J., and McEwen, B., "Three-dimensional microscopic light field particle image velocimetry," Experiments in Fluids 58(3), (2017).
[10] Wanner, S., and Goldluecke, B., "Variational light field analysis for disparity estimation and super-resolution," IEEE transactions on pattern analysis and machine intelligence 36(3), 606–619 (2014).
[11] Broxton, M., Grosenick, L., Yang, S., Cohen, N., Andalman, A., Deisseroth, K., and Levoy, M., "Wave optics theory and 3-D deconvolution for the light field microscope," Optics Express 21(21), 25418 (2013).
[12] Li, H., Guo, C., and Jia, S., "High-Resolution Light-Field Microscopy," presented at Frontiers in Optics, FW6D.3, (2017).
[13] Rossi, M., and Frossard, P., "Light Field Super-Resolution Via Graph-Based Regularization," arXiv preprint arXiv:1701.02141 (2017).
[14] Bishop, T.E., Zanetti, S., and Favaro, P., "Light field superresolution," in Comput. Photogr. ICCP 2009 IEEE Int. Conf. On, 1–9 (2009).
[15] Broxton, M., Grosenick, L., Yang, S., Cohen, N., Andalman, A., Deisseroth, K., and Levoy, M., "Wave optics theory and 3-D deconvolution for the light field microscope," Optics Express 21(21), 25418–25439 (2013).
[16] Cohen, N., Yang, S., Andalman, A., Broxton, M., Grosenick, L., Deisseroth, K., Horowitz, M., and Levoy, M., "Enhancing the performance of the light field microscope using wavefront coding," Optics Express 22(20), 24817–24839 (2014).
[17] Ng, R., Levoy, M., Brédif, M., Duval, G., Horowitz, M., and Hanrahan, P., "Light field photography with a hand-held plenoptic camera," Computer Science Technical Report CSTR 2(11), (2005).
[18] Ng, R., "Fourier slice photography," in ACM Trans. Graph. TOG 24, 735–744 (2005).
[19] Abrahamsson, S., Blom, H., Agostinho, A., Jans, D.C., Jost, A., Müller, M., Nilsson, L., Bernhem, K., Lambert, T.J., et al., "Multifocus structured illumination microscopy for fast volumetric super-resolution imaging," Biomedical Optics Express 8(9), 4135–4140 (2017).
[20] Hajj, B., Wisniewski, J., El Beheiry, M., Chen, J., Revyakin, A., Wu, C., and Dahan, M., "Whole-cell, multicolor superresolution imaging using volumetric multifocus microscopy," Proceedings of the National Academy of Sciences 111(49), 17480–17485 (2014).